Journal of Comparative Physiology A (2022) 208:405–420
https://doi.org/10.1007/s00359-022-01546-1

ORIGINAL PAPER

Morphology and receptive field organization of a temporal processing region in *Apteronotus albifrons*

John Leonard[1] · **Atsuko Matsushita**[2] · **Masashi Kawasaki**[1]

Received: 27 September 2021 / Revised: 4 February 2022 / Accepted: 4 February 2022 / Published online: 1 March 2022

Abstract

The timing system of weakly electric fishes is vital for many behavioral processes, but the system has been relatively unexplored in *Apteronotus albifrons*. This paper describes the receptive fields of phase-locked neurons in the midbrain of *A. albifrons*, in combination with neuroanatomy and electron microscopy (EM) to delineate a phase-locked area in this fish, the magnocellular mesencephalic nucleus (MMN). The MMN was isolated electrophysiologically through the detection of phase-locked field potentials of high amplitude. Single-cell recordings were made with a sharp electrode while a phase-locked modulated stimulus was provided to the fish. Receptive field centers of phase-locked neurons in MMN were consistent with tuberous electroreceptor density maps from previous studies, but no receptive field centers were found in the posterior 50% of the body. Intracellular and extracellular labeling of MMN revealed three cell populations: giant cells with large somata (19–24 µm) and their axonal arborizations which span across the entire extent of MMN, axon terminals from spherical cells of the electrosensory lateral line lobe (ELL), and small cell somata (3–7 µm) along with their projections which extend outside the nucleus. EM revealed multiple gap junction and chemical synapses within MMN. Our results indicate that MMN is a dedicated temporal processing center in *A. albifrons*.

Keywords Apteronotus · Temporal processing · Phase-locked neurons · MMN · Receptive field · Electric fish

Introduction

The brain uses several different coding modalities for transmitting information, such as rate coding, labeled-line coding, ensemble coding, and time coding (Gerstner et al. 1997; Konishi 2003; Somjen 1972). Time coding entails the transmission of information by utilizing the timing of action potentials rather than their frequency. Timing systems operate using comparable algorithms, as well as similar morphological and physiological features (Konishi 1991). Despite these similarities, there are often differences in the circuitry and anatomy of temporal processing areas in the brain that arise out of evolutionary necessity for behavioral capabilities, as seen when comparing the auditory systems of chickens and owls, who utilize temporal processing for sound localization (Carr and Friedman 1999).

Weakly electric fishes use a phase coding system in conjunction with a separate and parallel amplitude coding system for the purposes of electrolocation of prey, electrocommunication with conspecifics, species recognition, and sexual selection (Kawasaki 2009). In the wave-type genus *Eigenmannia*, this phase coding system is well documented, and consists of a network of neurons which fire action potentials phase-locked to the 300–600 Hz electric organ discharge (EOD) at a 1:1 ratio in both the peripheral and central nervous system (Rose and Heiligenberg 1985). In the case of the wave-type *Apteronotus* genus of electric fishes, the frequency of EOD discharge (f_{EOD}) can be higher than 1 kHz, which phase coding neurons have to match to maintain the 1:1 ratio seen in *Eigenmannia*. This higher frequency creates interesting questions as to how the temporal processing system may be different in these fish. While the amplitude encoding system has been well documented in *Apteronotus leptorhynchus* (Nelson and Maciver 1999; Bastian et al. 2002; Chacron et al. 2003; Maler 2009a, b; Martinez et al. 2016) and the phase encoding systems

✉ John Leonard
jl5jj@virginia.edu

[1] Department of Biology, University of Virginia, Charlottesville, VA, USA

[2] Department of Evolutionary Studies of Biosystems, SOKENDAI (The Graduate University for Advanced Studies), Hayama, Japan

of other weakly electric fishes have been well established (Carr et al. 1986a, b; Kawasaki and Guo 1996; Matsushita et al. 2013), there has been no in-depth characterization of the timing system, or central phase-locked neurons firing at high frequencies in the *Apteronotus* genus, and specifically in *Apteronotus albifrons*.

In this study, we investigated morphology and physiology of the central timing system of *A. albifrons* by combining neuroanatomical labeling techniques and neurophysiology using the field potential, extracellular, and intracellular recording techniques.

Materials and methods

Fish

We used 65 fish of *A. albifrons* (11–13 cm). The fish were acquired from a local dealer and kept in community tanks (2–7 fish per tank, 26–29 °C, 5–8 kΩ · cm). Fish were fed a daily diet of either live black worms or pellets (Xtreme Aquatic Foods). All animal procedures were approved by the University of Virginia Animal Care and Use Committee (Protocol# 1904).

Surgery

Prior to each experiment, the fish was anesthetized with MS-222 (1:10,000) and immobilized with an intramuscular injection of Flaxedil (gallamine triethiodide, 0.03%, 30–50 µl) before being intubated with a breathing tube which perfused aerated water over the gills (1 drop/s). Fish were placed in a foam-lined clamp and submerged in an experimental tank (26–29 °C, 5–8 kΩ · cm) such that water covered all but the parietal portion of the head. A silver wire electrode was placed underneath the head and a second U-shaped electrode surrounded the tail, which was held in place with a mesh platform. In this way, the EOD could be sampled and used for monitoring fish condition. A 2 × 3 mm area of skin and a 1 × 3 mm area of bone were removed, exposing the midbrain, and a plastic post was glued to the parietal bone for mechanical stability. The foam-lined clamp was then removed and the stimulus platform was placed around the fish.

Stimulus platform

A custom stimulus platform was constructed for this experiment. The platform consisted of two adjustable acrylic plates which fit into a frame underneath the fish. Each plate was roughly cut to match the curvature of the fish and held 12 stimulus electrodes and 1 reference electrode. The stimulus electrodes consisted of insulated silver wire, coiled into a corkscrew shape of 1 mm diameter at the tip and held in place with small pieces of plastic tubing, which also allowed for fine adjustments in electrode location. The reference electrodes consisted of two fixed screws which were partially submerged in the water. Stimulus electrodes were placed approximately 1 mm from the fish's skin and spaced approximately 0.5 cm apart in the head area, 1 cm apart in the mid-body area, and 2 cm apart near the tail. Reference electrodes were located at approximately mid-body and 5 cm from the fish's skin. All electrode wires were connected to a ribbon cable connector which led to a custom-built switch box, allowing for selection of individual electrodes and different electrode pairs (Fig. 1).

Stimulus

For recording action potentials and labeling of phase-locked neurons, no artificial stimulus was applied to the preparation. Neurons responded simply to fish's own EODs. For the receptive field measurements, a sinusoidal stimulus (1–10 mV/cm measured ~ 1 mm from the skin) that is frequency-clamped to f_{EOD} + 20 Hz, was created with a phase synthesizer (Wavetek 650). The addition of the stimulus to the natural EOD creates phase modulations at the level of the

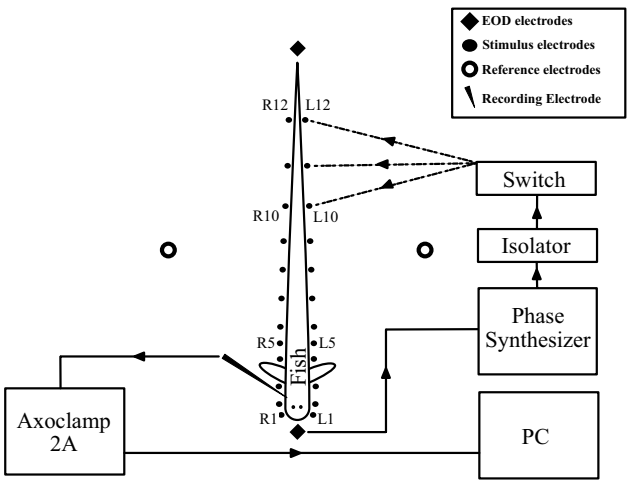

Fig. 1 Experimental setup for measuring receptive fields. An artificial sinusoidal stimulus is produced by the phase synthesizer and proceeds to an isolator and custom-built switch which controls which electrode pairs are used. *Diamonds* indicate the EOD recording electrodes which sample the fish's EOD for the phase synthesizer to produce a stimulus with a frequency of 20 Hz. *Closed circles* indicate the stimulus electrodes which deliver the artificial stimulus. Electrodes are lettered according to the side of the body (*R* for right, *L* for left), and numbered according to their longitudinal location along the fish's body (*1* as the most anterior electrode, *12* as the most posterior electrode). *Open circles* indicate the reference electrodes for the Left-side and Right-side stimulus configurations. *Dashed lines* indicate that the switch may be used to choose between different electrodes for stimulus delivery

electroreceptors, and are reflected in the phase modulation of recorded neurons. The depth of modulation in phase-locked neural responses was used as a measure for the neurons' receptive fields. The sinusoidal stimulus passed through an isolator and attenuator box before reaching the switch box. Three stimulus configurations were used: one of the left side electrodes vs right side reference electrode (termed "Left-side"), one of the right-side electrodes vs left-side reference electrode (termed "Right-side"), and two electrodes of right- and left-side straddling the fish (termed "Opposite"). For each configuration, a baseline recording of the EOD and neuron were taken without the sinusoidal stimulus, followed by one second of stimulation using each electrode, starting at the head, and progressing to the final electrode near the tip of the tail (L1–L12 and/or R1–R12 in Fig. 1).

Neurophysiological recording

Phase-locked neurons in the midbrain were first localized via field potential using a blunt tip glass capillary electrode (12 µm tip diameter) filled with 100 mM NaCl. Field potential amplitude varied from 1 to 3 mV. The electrode depth was measured from the cerebellar surface using a microdrive reading (Burleigh 6000). The electrode positioning and mapping of the target area were done using a reticle on the dissection microscope. EOD artifacts were canceled out of the field potential recordings by taking a reference sample below the brain surface, where no neural phase-locked potential is expected, and subtracting it from the field potential sample.

Intracellular potentials were recorded using a glass capillary electrode (tip diameter < 1 µm) filled with 1 M KCl. Electrode resistance was measured between 80 and 120 MΩ. Intracellular recording electrodes were positioned based on initial incursions using a broken-tip NaCl electrode. These initial incursions were used to define the depth and size of the area where phase-locked neurons could be found via the detection of their easily perceptible field potential. Field and intracellular potentials were recorded with Axoclamp 2A amplifier (Axon Instruments).

Any phase-locked neurons whose condition was maintained through the completion of all three stimulus configurations were included in the data. Any neurons which were not phase-locked, or which were lost during the experiment, or which did not yield decipherable data due to noisy traces were not included in the data.

Analysis

Recordings were analyzed using custom-built programs in Matlab. Intracellular spike raw data were processed using a custom-built filter and analyzed for the time differences

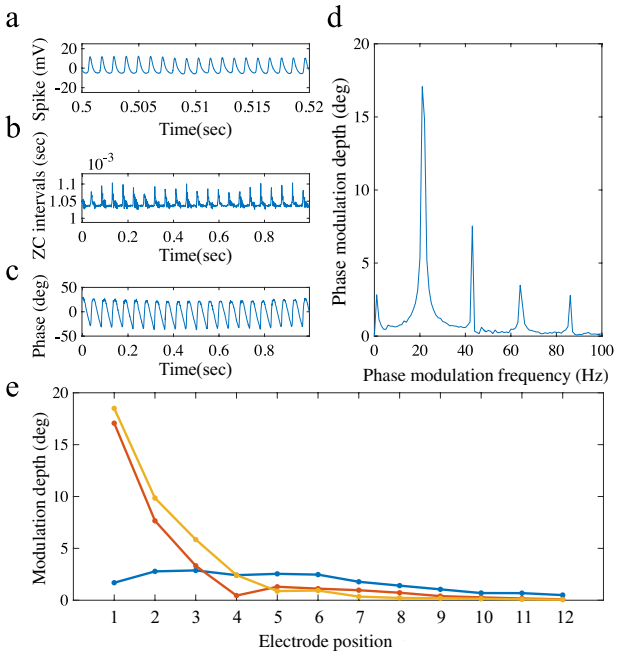

Fig. 2 Receptive field analysis in a single neuron. **a** The intracellular potential of an example neuron during a brief window of the recording time. **b** The zero-cross intervals from the same neuron during 1 s of stimulation. **c** The phase modulation of the neuron during stimulation. **d** The phase modulation spectrum of the neuron during stimulation. **e** The modulation depth of the neuron for Left-side (blue), Right-side (yellow), and Opposite (red) electrode configurations

(intervals) in zero-cross events, the time at which the voltage crosses from negative to positive, between each spike (Fig. 2a and b). Zero-cross events were detected if the following conditions were met:

$$\mathrm{Ys}(i-1) * \mathrm{Ys}(i) < 0 \& \mathrm{Ys}(i-1) < 0,$$

where $\mathrm{Ys}(i)$ is the voltage measurement at the ith sample.

To capture zero-cross times occurring in between samples, the zero-cross times were calculated using interpolation with the following equation:

$$\mathrm{zct} = (i-1) * \mathrm{int} + \mathrm{int} * \frac{|\mathrm{Ys}(i-1)|}{\mathrm{Ys}(i) - \mathrm{Ys}(i-1)},$$

where zct is the zero-cross time, int is the interval, and Ys is the voltage measurement.

A cumulative sum of zero-cross time differences was used to calculate the mean interval using the equation:

$$\bar{x}_{\mathrm{int}} = \frac{\mathrm{zct}_{\mathrm{end}} - \mathrm{zct}_1}{\mathrm{length}(\mathrm{zct}) - 1},$$

where $\mathrm{zct}_{\mathrm{end}}$ and zct_1 are the last and first data points in the cumulative sum of zero-cross time differences respectively, and $\bar{x}_{\mathrm{int}}$ is the mean interval.

The mean interval was then used to create a constant time reference (i.e., the time the next spike is expected if there is no phase modulation) using the equation:

$$t_{\mathrm{ref}}(i) = \mathrm{zct}_1 + \bar{x}_{\mathrm{int}} * (i-1).$$

The time modulation was then obtained using the equation:

$$t_{\mathrm{diff}} = \mathrm{zct} - t_{\mathrm{ref}}.$$

The phase modulation (Fig. 2c) was then obtained from the zero-cross data using the following equation:

$$P_{\mathrm{diff}} = \frac{t_{\mathrm{diff}}}{\bar{x}_{\mathrm{int}} * 360},$$

where P_{diff} is the phase difference, t_{diff} is the change in zero-cross time, and $\bar{x}_{\mathrm{int}}$ is the mean interval.

The phase modulation data were then processed using Fast Fourier Transform, which uses the following Discrete Fourier Transform equation for X of length n:

$$Y(k) = \sum_{j=1}^{n} X(j) W_n^{(j-1)(k-1)},$$

where $W_n = e^{(-2\pi i)/n}$ is one of n roots of unity.

The data were then viewable as a phase modulation spectrum where the amplitude of different modulation frequencies could be seen (Fig. 2d). Integration of the phase modulation spectrum revealed the total depth of modulation seen while providing the stimulus using each individual electrode (Fig. 2e). This methodology has been successfully used previously for phase-locked neuronal analysis, as the zero-cross times track phase shifts in stimuli (Guo and Kawasaki 1997). Zero-cross analyses were applied to describe receptive fields, as stimuli within a receptive field will produce shifts in zero-cross times at an expected modulation frequency, while stimuli outside of it will not.

Receptive field centers were defined as the body location adjacent to the electrode which elicited the greatest magnitude of phase modulation. Receptive field size (width) was defined as the body area adjacent to electrodes which produced greater than 50% of the peak modulation. Left vs right side receptive field location was determined by comparing the magnitudes of the peak modulation between each stimulus configuration.

Zero-cross analysis was also used to examine the jitter of phase-locked neurons. For jitter analysis, we included 65 neuronal recordings in the absence of an artificial stimulus, which met the aforementioned inclusion criteria. For these recordings, zero-cross times were obtained to calculate the spike intervals. Using the same process which was used in calculating the phase modulation above, the cumulative sum of the intervals was then taken to produce a constant time reference (i.e., the time the next spike is expected if there is no jitter). Jitter was then calculated using the following equation:

$$\mathrm{Jitter} = S\left(\mathrm{zct} - t_{\mathrm{ref}}\right),$$

where zct is the zero-cross time, t_{ref} is the constant time reference, and S is the standard deviation.

Anatomy

For simultaneous intracellular recording and labeling, glass-capillary electrodes (tip diameter < 1 µm) were filled with 2% biocytin (Sigma B4261) in 1 M KCl and iontophoresed at 1 nA for 2–10 min. For extracellular labeling of many neurons, we used glass-capillary electrodes (tip diameter ~ 12 µm) filled with 2% biocytin (Sigma B4261) in 1 M KCl and iontophoresed at 6 µA for 5–30 min. Fish survival time before perfusion ranged from 1 to 4 h for intracellular injection and 2–6 h for extracellular injection. Fish were transcardially perfused with a physiological solution and then a fixative solution (2% paraformaldehyde (PFA) and 2% glutaraldehyde (GA)) in 0.1 M phosphate buffer (PB, pH = 7.4). Following perfusion, the brain was removed and placed in the fixative solution overnight at 4 °C. Transverse sections were sliced at 60 µm (Leica model VT1000S). Sections were rinsed in phosphate buffer saline (PBS, 0.02 M PB with 0.9% NaCl) and treated with 0.5% hydrogen peroxide (H_2O_2) in PBS to use up any endogenous peroxidase. The sections were then soaked at room temperature overnight in PBS with an avidin–biotin complex (ABC, Vector Laboratories PK-6100) and 0.3% Triton X-100. Sections were then washed in 0.02 M PB and subsequently soaked in 0.2 M PB with 0.05% diaminobenzidine (DAB) and 0.04% nickel ammonium sulfate for 10 min. Sections were then reacted with 0.002% H_2O_2 for 1–2 min. The sections were then mounted on slide-glass, counterstained with neutral red, and dehydrated with an ethanol series before being cleared using HemoDe (Fisher Scientific) and sealed with Permount (Fisher Scientific).

Light microscopy (LM) observations were performed using a BH-2 (Olympus) microscope. Composite micrographs were made using Affinity Designer and the e-Tiling focus-composition software (Mitani Corporation). For camera lucida drawings, composite micrographs were made, and neurons were traced using a drawing tablet (Wacom Intuos), before a composite image was produced within Affinity Designer while referencing section continuity using the microscope.

For conventional electron microscopy (EM) and semithin LM, we followed Matsushita and Kawasaki (2004). Briefly, after anesthetization, fish were perfused with 2% PFA and

2% GA in 0.1 M PB, and the brain was subsequently postfixed in the same fixative for 4–16 h. For vibratome sectioning, isolated brains in PBS were embedded in 35% (*w*/*v*) gelatin and then sliced with a vibratome at 80–100 µm (80 µm for MMN, 100 µm for other parts) thickness. Floating sections stored in 0.02 M PBS were heated at ~ 36 °C to remove gelatin. The sections of the MMN region were picked up and sandwiched between pieces of papers (#54 Whatman) to avoid wrinkling. The sandwiched sections (hereafter simply 'sections') were transferred to 0.1 M sodium cacodylate buffer (CB pH 7.3). Then, the sections were postfixed with 0.1% OsO_4 (osmium tetroxide) in 0.1 M CB for 30–40 min at room temperature, briefly rinsed with water, dehydrated with a graded ethanol series (50, 70, 80, 90, 95, 100, 100%) at 10 min each, infiltrated with propylene oxide (3 × 10 min), and flat-embedded in Quetol 812 (Nisshin EM) between two sheets of OHP film. We prepared two types of embedding media Quetol 812: "regular" type and "soft" type recipes for EM and LM observation, respectively. Even numbered sections of the MMN were embedded in the regular media, and odd numbered sections were embedded in the soft media. Semithin sections from both soft- and regular-resin-embedded blocks were made on an ultramicrotome (Leica UCT) with a diamond histo-knife, stained with 0.1% Azure II. Ultrathin sections mounted on nickel grids, double stained with 4% uranyl acetate and 0.4% lead citrate, were examined with a transmission electron microscope (H7650, Hitachi) equipped with a digital camera (Quemesa, Olympus).

For EM observation of biocytin labeled sections, floating sections of the MMN region made with a vibratome were first rinsed in 0.02 M PB with 0.9% NaCl (PBS), treated with 0.5% hydrogen peroxide (H_2O_2) in PBS for 15 min, and soaked in PBS containing ABC (Vector Laboratories PK-6100) and 0.05% Triton X-100 for 18–21 h at room temperature. After being rinsed with 0.02 M PB, the sections were presoaked in 0.1 M PB containing 0.05% diaminobenzidine (DAB) and 0.04% nickel ammonium sulfate for 10 min, and then reacted with 0.003% H_2O_2 for 2 min. Wet sections were observed for a quick check with a light microscope (BX-51, Olympus) equipped with a DP74 camera system. EFI (extended focus imaging) image processing function (cellSens standard, Olympus) was used for *z*-axis projection imaging. The sections were then processed as above for embedding in Quetol 812 media with the 'regular' recipe with the exception that 0.1 M PB was used for all steps instead of CB.

Results

1:1 Firing of phase-locked midbrain neurons

We obtained sharp electrode intracellular recordings from individual cells within the midbrain. Subject fish EOD frequency measurements ranged from 904 to 1340 Hz (Fig. 3). In total, 80 midbrain neurons were recorded from and identified as being phase-locked to the EOD at a 1:1

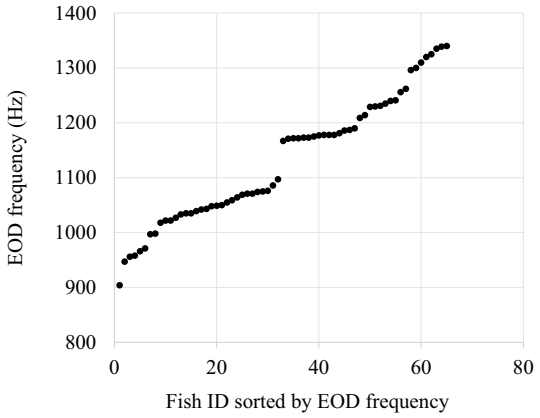

Fig. 3 Distribution of EOD frequencies measured in subject fish

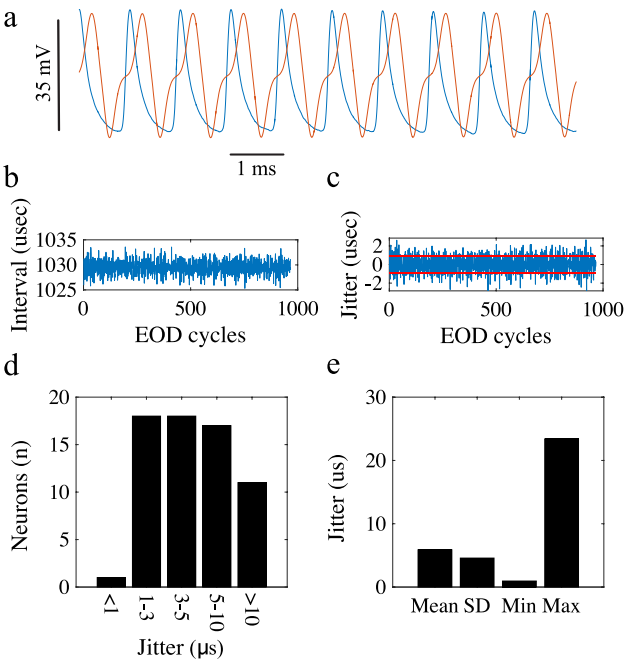

Fig. 4 Jitter analysis. **a** Intracellular potential over time from a single neuron in MMN showing 1:1 phase-locking of the neuron (blue) to the EOD (orange) with no artificial stimulus present. The EOD shown is normalized to the amplitude of the neuron. The vertical scale bar applies to the neuron only, while the horizontal scale bar applies to both neuron and EOD. **b** The intervals between subsequent action potentials over the course of consecutive EOD cycles for the same neuron from (**a**) (f_{EOD} = 971 Hz). **c** The jitter over the course of consecutive EOD cycles for the same neuron from (**a**). *Horizontal red lines* indicate the bounds of one standard deviation, which was used for the jitter values in (**d**) and (**e**). The jitter value for this neuron was 0.95 µs. The jitter value for the EOD was 1.03 µs. **d** The distribution of jitter for all neurons measured (n = 65). **e** The mean, standard deviation, minimum, and maximum jitter values for all neurons measured

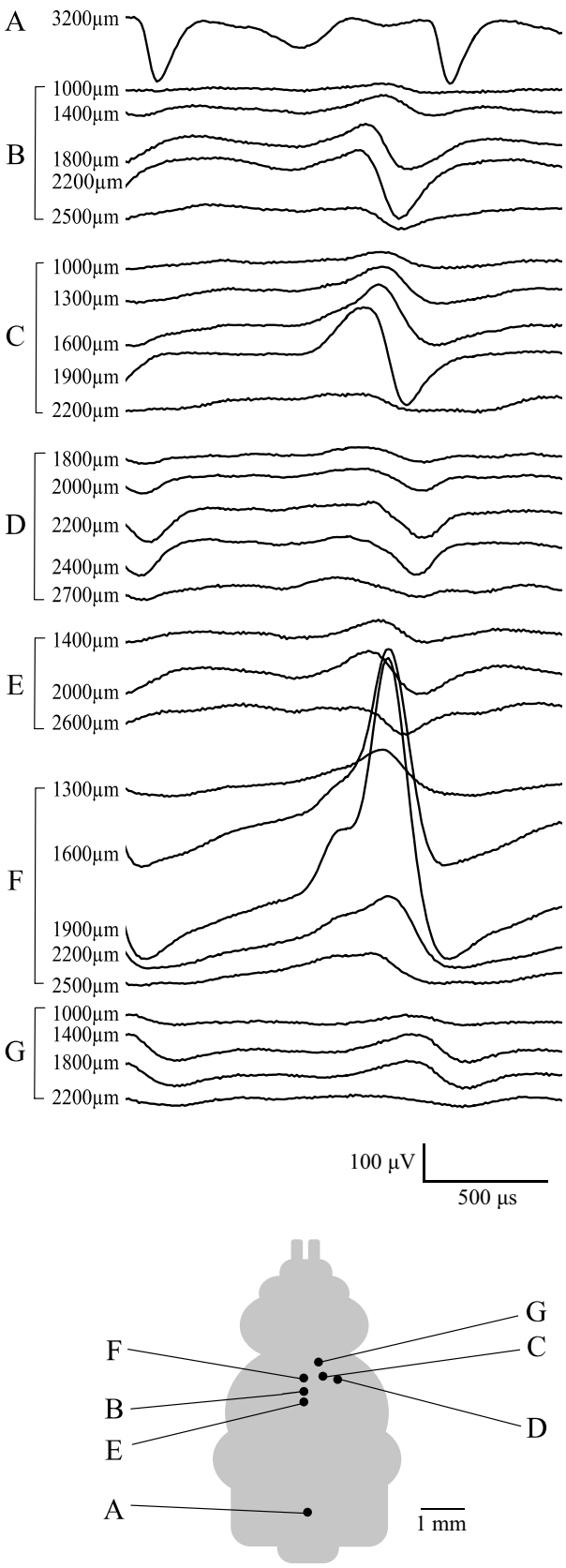

Fig. 5 Field potential and intracellular recordings in the lateral lemniscus decussation (dLL) and torus semicircularis (TS). Each letter on the left side of the chart corresponds to a recording location shown on the dorsal view of the brain at the bottom. The left brackets denote which traces correspond to each letter. Each number beside the letters denotes the corresponding depth for each recording trace as measured from the surface of the cerebellum. The recording sites are as follows: ***A*** denotes the decussation of the lateral lemniscus, ~ 3 mm posterior to the anterior origin of the cerebellum, ***B*** is on the midline of TS, ~ 300 µm posterior to the anterior origin of the cerebellum, ***C*** is ~ 200 µm lateral and ~ 200 µm anterior to ***B***, ***D*** is ~ 200 µm lateral and ~ 200 µm posterior to ***B***, ***E*** is ~ 400 µm posterior to ***B***, ***F*** is ~ 500 µm lateral to ***B,*** and ***G*** is ~ 200 µm lateral to ***B***

ratio (Fig. 4a). These neurons ranged in firing frequency from roughly 900 Hz to 1.3 kHz. Jitter was measured in 65 of the phase-locked neurons with no artificial stimulus present. In this way, the neuronal jitter could also be compared with the EOD jitter. No significant correlation between EOD jitter and neuronal jitter was found. The mean neuronal jitter found in these fish was 5.9 µs with a standard deviation of 4.6 µs. The minimum jitter found was 0.9 µs and the maximum jitter found was 23.4 µs (Fig. 4b–e). 35 phase-locked midbrain neurons which met the inclusion criteria were also recorded from and analyzed for receptive field organization (see "Materials and methods").

Field potential

To examine the distribution of phase-locked neurons in the brain, field potentials phase-locked to the EOD in the absence of an artificial stimulus were recorded in the decussation of the lateral lemniscus (dLL), and torus semicircularis (TS) (Fig. 5). The field potentials were large (up to 2.5 mV) and highly constant in amplitude over cycles of repetitive waveform, indicating that individual potential sources were firing in synchrony. Positive and negative deflections in recording traces were seen at multiple recording locations, with increasing latency moving from dLL to various parts of TS. Negative deflections in both lateral and medial TS were delayed by 750 µs and more than 900 µs relative to the negative deflection in dLL, respectively. Negative deflections in posterior and anterior TS were delayed by ~ 850 µs and ~ 950 µs, respectively. Recordings from individual phase-locked cells in medial TS were delayed by ~ 800 µs relative to dLL. Field potential amplitudes were greatest near the midline of the anterior midbrain at 2 mV, and decayed both rostro-caudally, and laterally, highlighting a well-defined area of phase-locked activity centered around the midline of anteromedial TS. A shallower band of field potential phase-locked to the EOD was also found lateral to the main area of phase-locked activity. The recording depths at which phase-locked field potentials were detected included a band of 1.2 mm in depth from 1300 to 2500 µm where the amplitude was the largest (location *F* in Fig. 5),

and shallower bands surrounding it which encompassed some of the same depths. Included among these were a 400 µm thick area of field potential from 1400 to 1800 µm, seen ~ 500 µm posterior to the field potential maximum location (location *E* in Fig. 5), and a 1200 µm thick area from 1000 to 2200 µm seen 300 µm lateral to the field potential maximum location (location *C* in Fig. 5). Relative to the field potential maximum, recordings 300 µm laterally and 300 µm anteriorly or posteriorly revealed a 400 µm band from 1400 to 1800 µm and a band of ~ 1100 µm from 1400 to 2500 µm, respectively (locations *G* and *B* in Fig. 5). Finally, ~ 500 µm lateral to the field potential maximum we found a band of ~ 400 µm from 2000 to 2400 µm (location *D* in Fig. 5). Recordings from individual neurons yielded traces whose timing aligned with the field potential from that location.

Neuroanatomy

Semi-thin transverse sections of the recording areas of the midbrain revealed a large unpaired midline structure which was clearly distinguished from the surrounding TS by a high density of large diameter myelinated fibers (Fig. 6a). In comparing the semi-thin sections to the field potential recordings, we saw that wherever there was a high density of large diameter fibers, we detected the greatest magnitude of field potential. Extracellular biocytin injection into the field potential recording area directly after the recording process confirmed the recording location within this structure (location *F* in Figs. 5 and 6b). In addition to the density of large diameter axons, we found sparse occurrences of large diameter somata of giant cells within these same locations (Fig. 6c). We call this area the magnocellular mesencephalic nucleus (MMN), because it shares many features with the MMN of low-frequency pulse-type gymnotiform fishes (Réthelyi and Szabo 1973; Matsushita et al. 2013).

The MMN of *A. albifrons* began centered on the midline of anterior TS, just posterior to the forebrain, and continued posteriorly for approximately 500 µm before yielding any remaining space to TS. Its dorsal origin was located just beneath the torus longitudinalis (TL) at approximate depths of 500–750 µm measured from the ventral border of the cerebellum and extended down to the pretectal bundle. MMN shape and dimensions were somewhat variable between individual fish. Across eight fish, the mean longitudinal length was 570 µm, with a mean maximum width and maximum height of 950 µm and 840 µm, respectively. The mean minimum width and minimum height were 380 µm and 400 µm (Table 1). These dimensions changed along the anterior–posterior axis. One fish measured 875 µm in width and 500 µm in height at the most anterior portion. Moving posteriorly, it reached 1 mm in width and 750 µm in height at its largest point before changing in shape to a taller and thinner modality, reaching 900 µm in height and 500 µm in width at its tallest point. Continuing posteriorly, the region shrunk in size until reaching a width of 400 µm and a height of 400 µm. The structure then transitioned to a layer-like modality for 120 µm before yielding the space entirely to TS. Additionally, there were two bilateral horn-like protuberances, approximately 100 µm in depth, made up of similar large diameter, heavily myelinated fibers which extended

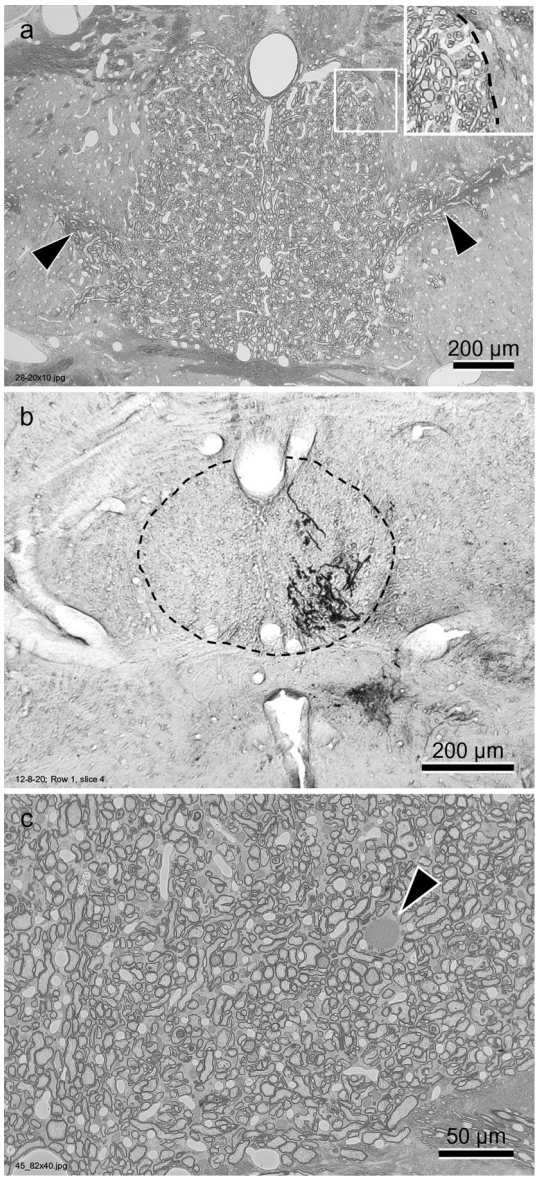

Fig. 6 Transverse sections of the magnocellular mesencephalic nucleus (MMN). **a** A semithin section of the entire MMN. The borders can be differentiated by the change to a high density of large diameter fibers (*boxed area*, enlarged in *inset*). *Arrowheads* indicate the locations of the horns of MMN (hMMN). **b** Labeled recording site of phase-locked field potentials within MMN. *Dashed line* indicates the boundaries of MMN. **c** Semithin section of a portion of MMN with a giant cell soma (*arrowhead*)

roughly 300 µm laterally from MMN. We are calling these protuberances the lateral horns of MMN (hMMN) (Fig. 6a).

Intracellular injection of biocytin into individual thick fibers within the MMN revealed that some of the fibers belonged to the giant cells, while other fibers were axons of the spherical cells in the electrosensory lateral line lobe (ELL). Additionally, a third type, small cells, were retrogradely labeled via extracellular injection of biocytin into TS near hMMN.

Spherical cells

Extracellular biocytin injection into dLL labeled spherical cell terminals in MMN and retrogradely labeled spherical cell somata in ELL. Somata were seen in lamina I of the lateral, centrolateral, and centromedial segments of ELL, and were predominantly spherical in shape, with diameters of 12–15 µm (Fig. 7a). The initial segments of the cells were less than 1 µm in diameter, proceeding dorsomedially through ELL for ~ 100 µm before thickening to 1–2 µm (Fig. 7b). The axons continued in a dorsomedial direction until coalescing into thick bundles and crossing the midline contralaterally at the decussation of the lateral lemniscus. From there, the bundles moved dorsolaterally (Fig. 7c) before some of the axons exited the bundle, making a sharp turn before moving dorsomedially at the ventral margin of TS. Other axons advanced further dorsolaterally before making a sharp turn and moving into TS. The thicker axons continued dorsomedially through TS before making a sharp turn medially, entering hMMN. Other axons, mostly smaller in diameter at 2 µm or less, continued dorsally before terminating in various parts of TS outside of MMN (Fig. 7d). Axons within hMMN were found to be 1–4 µm in diameter. The axons then followed the horns into MMN before bilaterally terminating within MMN itself (Fig. 7e). Spherical cell terminals were seen in every area of MMN, with no terminals outside the nucleus, with the exception of the midline of anterior MMN, which was void of any spherical cell axons or terminals (Fig. 7f). Both terminals and axons could be found along the midline of the posterior ending of MMN, roughly 400 µm posterior to the forebrain-midbrain boundary. The axons thickened before terminating, and nearest the terminals were found to be as large as 10 µm. The axons then thinned to 1 µm or smaller and coiled into calyx-like endings (Fig. 7g). In some cases, a labeled spherical cell fiber was found to terminate on a giant cell soma (Fig. 7h).

Giant cells

Giant cell somata were found throughout MMN, and spatial distribution of their somata was somewhat variable between fish, but they were predominantly arranged along the lateral and ventral edges of MMN in the anterior sections, with a few somata found more centrally in posterior MMN. Giant cell somata were also found within hMMN, and within the most posterior portion of MMN where it transitions to a layer-like structure. The number of giant cell somata was variable between fish and found to be approximately 80 (Table 1). Intracellular biocytin injections of single units showed adendritic giant cell somata 19–24 µm in diameter with branching fibers 1–15 µm in diameter that were fully contained within MMN (Fig. 8a–c). Fiber thickness was not constant for most branches. Labeled giant cells extended their processes across the midline and throughout the entire width and depth of MMN. The initial axonal segments of the giant cells were found to be abruptly thin at ~ 1 µm in diameter, before suddenly thickening to 3–5 µm (Fig. 8d). After the initial segment, giant cell axons often made a hairpin turn before proceeding in the opposite direction. Axons then bifurcated many times and both thickening and thinning of

Table 1 Giant cell counts and MMN dimensional measurements across eight fish

Subject	Approximate dimension of the MMN					
	# of giant cell somata	Longitudinal length (µm)	Max width (µm)	Max height (µm)	Min width (µm)	Min height (µm)
Fish 1	64	540	1000	900	400	400
Fish 2	80	600	900	800	350	300
Fish 3	86	720	1000	900	400	400
Fish 4	77	660	900	800	300	400
Fish 5	86	480	900	800	400	400
Fish 6	87	540	800	800	500	400
Fish 7	94	600	1100	900	400	500
Fish 8	76	420	1000	800	300	400
Mean	81	570	950	840	380	400

Cell counts were performed under light microscopy. Measurements of dimensions were assessed under light microscopy as well as imaging done under light microscopy, and reflect the distances between the borders where there is a high density of thick, myelinated fibers on one side only

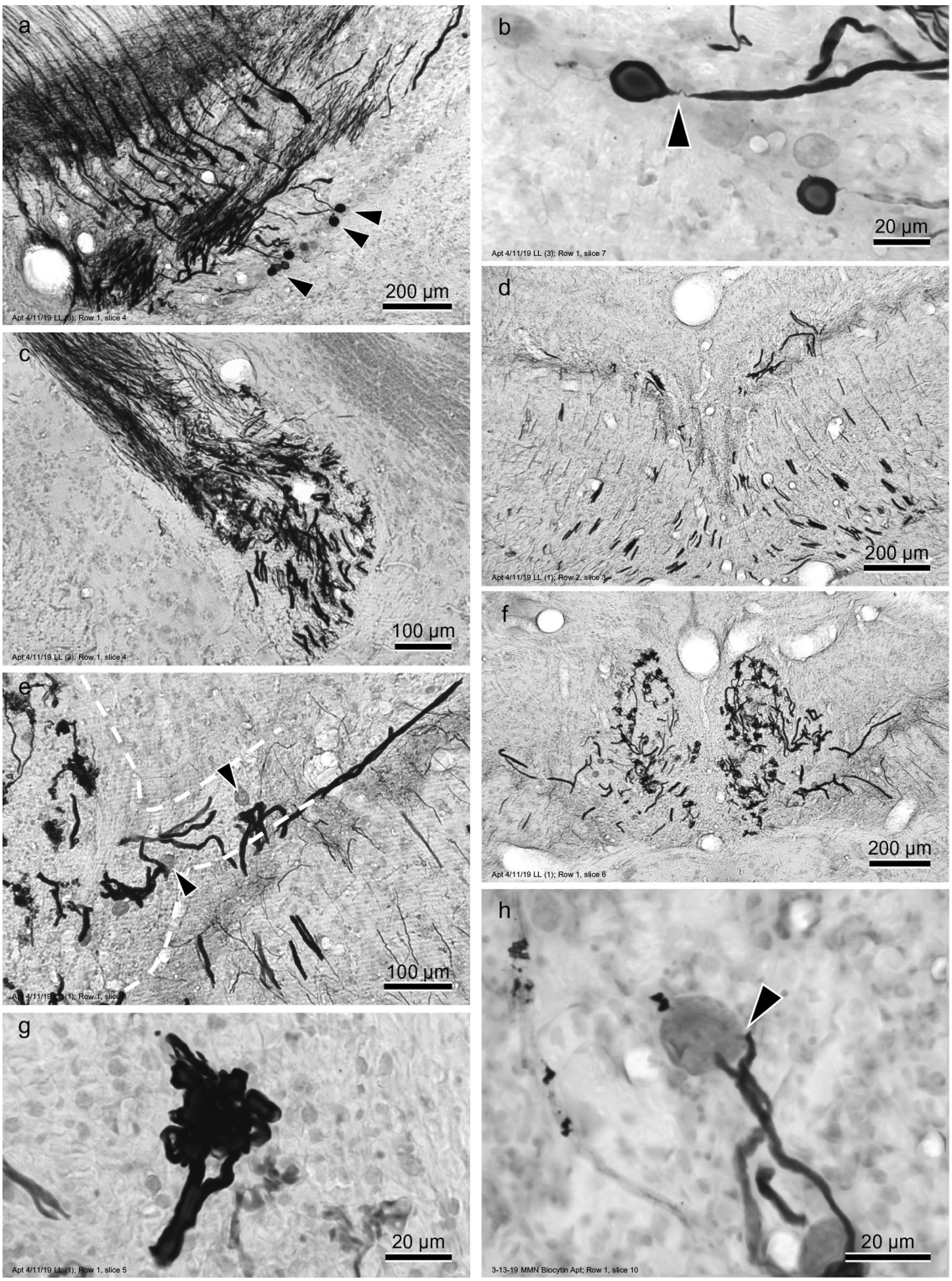

Fig. 7 Morphology of spherical cells. **a** Somata (*arrowheads*) and fibers of spherical cells (and fibers of pyramidal cells) labeled via extracellular injection of biocytin into dLL. **b** Spherical cell soma and initial axon segment. *Arrowhead* indicates thinning seen at the axon hillock. **c** Fiber bundle from ELL just prior to entering TS. **d** Fibers from ELL entering TS and moving towards MMN. **e** Spherical cell projections entering MMN via hMMN (*dashed lines*). Some giant cell somata can be seen within hMMN (*arrowheads)*. **f** Transverse section of MMN and hMMN with labeled spherical cell terminals. **g** Spherical cell terminal featuring a glomerulus-like structure. **h** Spherical cell fibers terminating in close proximity to giant cell soma (*arrowhead)*

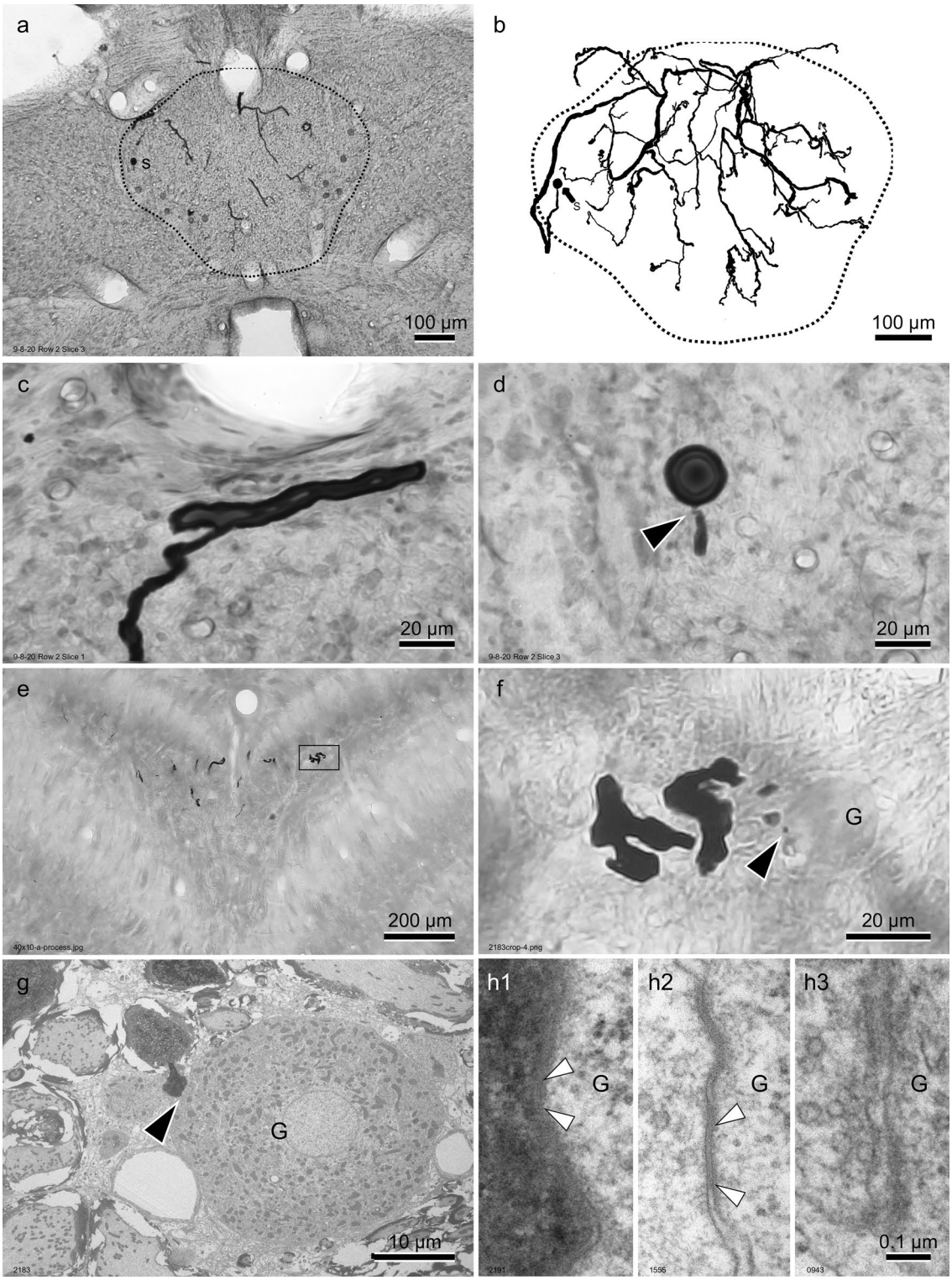
a
s
100 µm
9-8-20 Row 2 Slice 3
b
s
100 µm
c
20 µm
9-8-20 Row 2 Slice 1
d
20 µm
9-8-20 Row 2 Slice 3
e
200 µm
40x10-a-process.jpg
f
G
20 µm
2183crop-4.png
g
G
10 µm
2183
h1
G
2191
h2
G
1555
h3
G
0,1 µm
0943

◂**Fig. 8** Morphology of giant cells. **a–d** A giant cell intracellularly labeled with biocytin. **a** One of the sections containing the soma (s) enlarged in **d**. *Dotted line* indicates the borders of MMN. **b** A camera lucida drawing of the giant cell (s) featured in **a**. **c** A large fiber from the cell (s) featured in **a**. **d** The soma and initial axon segment of the cell featured in **a**. *Arrowhead* indicates the thin portion of the initial axon segment. **e** A transverse section through MMN featuring a giant cell labeled with biocytin through extracellular injection. *Boxed area* is shown in **f** under higher magnification. **f** A magnified view of the box in **e**. *Arrowhead* indicates a point of contact between the labeled giant cell terminal bouton and a non-labeled giant cell soma (G). **g** Electron micrograph (EM) from the adjacent section shown in **f**. The presynaptic fiber is heavily myelinated up until the final portion of the terminal. The contact (*arrowhead*) is enlarged in **h1** and is the site of an axosomatic synapse. **h1–h3** Synapses onto a giant cell soma. **h1** Gap junction-like structure (pair of *arrowheads*) between labeled bouton of the giant cell and a soma of a non-labeled giant cell. **h2**, **h3** Conventional EMs showing gap junctions (**h2**) and chemical synapse (**h3**), onto a giant cell soma (G). A pair of arrowheads indicate the gap junction between the terminal bouton and soma (**h2**)

the projections were seen as the fibers terminated throughout the majority of MMN. In one instance, a labeled giant cell fiber was found to contact a contralateral giant cell soma (Fig. 8e, f). Electron micrographs of the synapse region indicated gap junctions (Fig. 8g, h) as well as chemical synapses (Fig. 8h). Generally, we found that giant cell somata are proximal to heavily myelinated pre-synaptic fibers, some of which lose their myelin ~ 1 µm before synapsing onto the giant cell soma.

Small cells

An extracellular biocytin injection made ~ 300 µm lateral to MMN and proximal to hMMN retrogradely labeled a number of small cells within MMN (Fig. 9). The somata were numerous, measuring 3–7 µm in diameter, and were all found on either side of MMN at all depths (Fig. 9a), but were not found on the midline. Each small cell had two processes: an axon, and a single dendrite which does not bifurcate (Fig. 9b). Much like the spherical cells and giant cells, their initial segments were thin (< 1 µm) and abruptly thickened to 1–2 µm distally, probably due to myelination. Dendrites were 10–20 µm in length and were found in various directions and orientations. Axons immediately proceeded dorsolaterally or ventrolaterally in the direction of hMMN (Fig. 9c). Dendrites were seen in the form of a tufted dendritic tip (Fig. 9b, d). Electron micrographs revealed axosomatic synapses (Fig. 9d) which appear to be gap junctions (Fig. 9e, f). The dendritic tip area shows mixed synapses (Fig. 9g, h).

Receptive field centers

All 35 receptive field centers were found within the anterior 50% of the body length. Analyses showed that 45.7% of receptive field centers were found using the most anterior electrode, near the most anterior portion of the head, and the incidence of receptive field centers steadily decreased with increasing distance from the snout (Fig. 10a). In 34 of the 35 neurons, the peak response on one side was significantly larger than that on the opposite side. We determined that the receptive field resided on that side of the body for these neurons. In one neuron, the peak responses from both sides were indistinguishable indicating that electroreceptors for this neuron resided on the sagittal plane on the body surface.

Receptive field shape and size

Receptive fields were analyzed for one dimensional shape and size in the longitudinal axis. Receptive field tuning curves were diverse, but generally bell shaped and skewed towards one side, with decreasing responses seen up to a few electrodes away from the receptive field center (Fig. 2e). While no receptive field centers were found in the posterior half of the body, some receptive fields did extend to the posterior trunk. Electrodes in the posterior 50% of the body area elicited responses in only 7.49% of receptive fields or less on average, and no receptive fields were discovered to be contained within the space of the most posterior electrode (Fig. 10b). In terms of receptive field size, the mean width of receptive fields was found to be elicited by 4.7 electrodes for the left side configuration, 5.4 electrodes for the right-side configuration, and 3.5 electrodes in the opposite configuration (Fig. 10c). For most receptive fields this was roughly 2–3 cm in length, dependent upon the anatomical location of the RF center, as electrode spacing increases towards the tail (Fig. 1). The variance of receptive field width was found to be 6.3, 9.5, and 1.3 electrodes for left, right, and opposite configurations, respectively.

Discussion

Our results demonstrate that *A. albifrons* has a midbrain area, MMN, with strong field potentials phase-locked to the EOD at a 1:1 ratio. We also found individual neurons within MMN phase-locked to the EOD at a 1:1 ratio. Through extracellular injection of biocytin at field potential recording sites, and intracellular injection of recorded single-units, we were able to confirm that the phase-locked activity area corresponds to a region that exhibits large diameter myelinated fibers and large diameter somata. Examination of cell types within MMN revealed three varieties: spherical cell terminals, giant cell somata and axons, and small cell somata, axons, and dendrites.

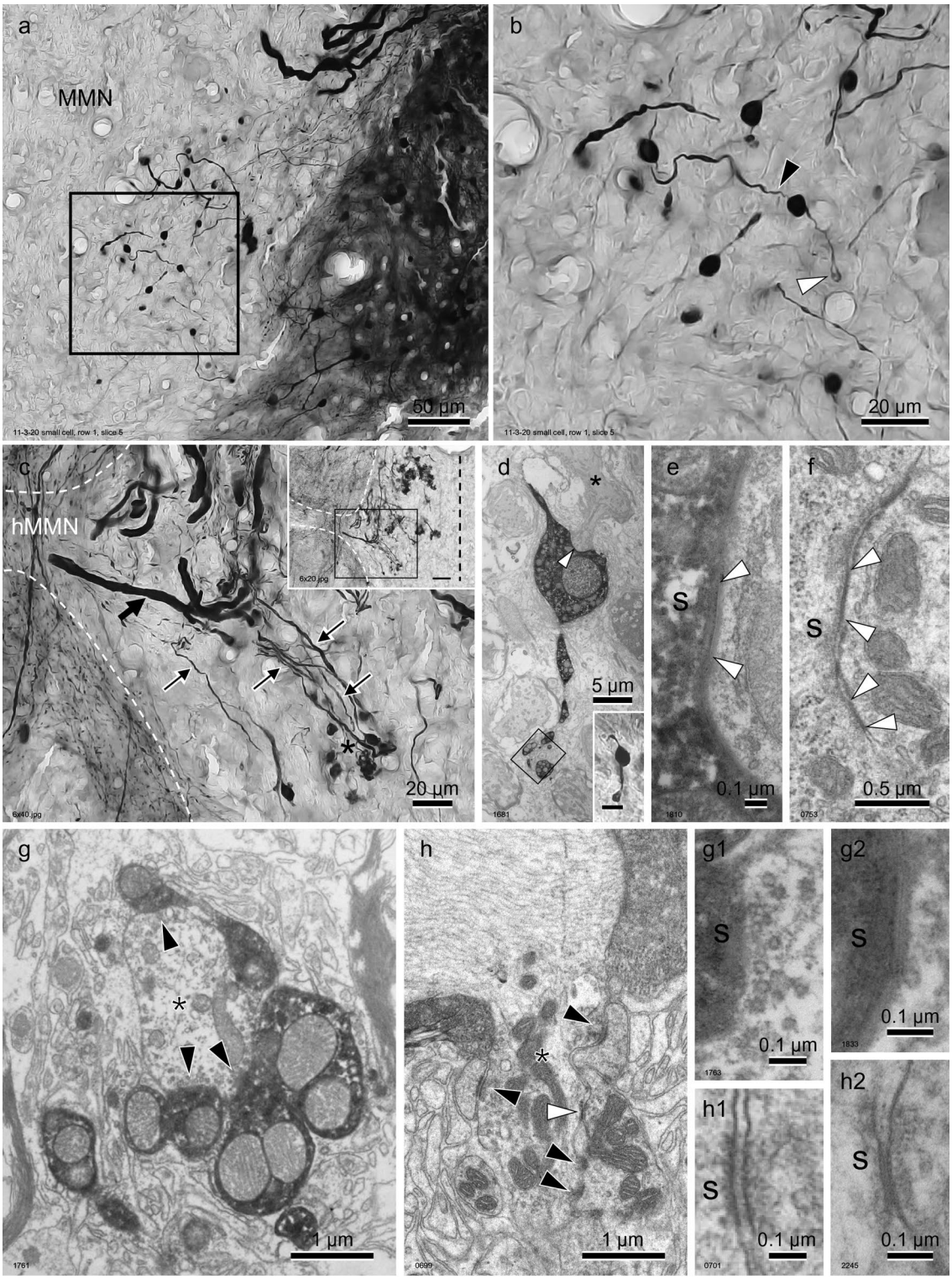

Receptive field analyses from intracellular recordings in MMN revealed receptive field centers only in the anterior 50% of the body, with a strong concentration in the head area.

1:1 firing of phase-locked neurons in the midbrain

1:1 phase-locking was confirmed within MMN via both intracellular and extracellular recordings (Figs. 1, 2, 3, 4, 5). This is notable considering the very high f_{EOD} of

◂**Fig. 9** Morphology of small cells. **a** Small cell somata and fibers labeled via extracellular biocytin injection outside of MMN (dark area on the right of the panel). *Boxed area* is shown in **b** under higher magnification. **b** Close up of small cells. A small cell is bipolar with a long axon (*black arrowhead*) and a dendrite, typically 10–20 µm in length, whose tip appears to be tufted (*white arrowhead*). **c** Biocytin labeled small cell somata and fibers, as well as spherical cell axons. A cluster of small cells (*asterisk*) send thin axonal projections (*arrows*) towards hMMN (outlined with *white-dashed lines*). Spherical cell fibers can simultaneously be seen entering MMN via hMMN (*thick arrow*). *Inset* shows a broader view of the area in relation to the midline (*black dashed line*). **d** A small cell labeled by extracellular injection of biocytin with axon and tufted dendritic tip. The concave portion of the soma (*white arrowhead*) is attached to a bouton of a thick axon (*asterisk*). The attachment is enlarged in **e**. The tufted tip (*boxed area*) is shown in **g** of a different consecutive section. *Inset* LM of this small cell showing morphology of the entire cell. The LM was taken before ultra-sectioning for EM. **e** EM of axosomatic synapse (*arrowhead* in **d**) onto small cell soma (s). Gap junction-like structure is indicated by a pair of *arrowheads*. **f** Conventional EM showing gap junctions between a small cell soma (s) and bouton. One gap junction is indicated by a pair of *arrowheads*. **g** EM of the tufted dendritic tip of the labeled cell from **d** with different consecutive sections. The small cell dendritic tip is characterized by numerous mitochondria compared to presynaptic profile (*asterisk*). *Arrowheads* indicate chemical synapses, and one of which is enlarged in **g1**. In other different consecutive sections of the dendritic tip, gap junction structure can be seen (**g2**) **h** Conventional EM showing a bouton *en passant* of a thick axon (*asterisk*) contact with a cluster of small postsynaptic portions, which is probably the dendritic tip of a small cell. *Black arrowheads* indicate chemical synapses, one of which is enlarged in **h1**, and a *white arrowhead* indicates a gap junction (enlarged in **h2**)

A. albifrons, and exhibits some differences to other high-frequency time coding systems. For example, neurons in the auditory system of the barn owl are capable of phase-locking to high-frequency auditory stimuli (1–8 kHz), but do not fire 1:1 with the stimulus (Sullivan and Konishi 1984). The 1:1 phase locking in *A. albifrons* is demonstrative of the importance of accuracy in this system, as 1:1 firing at ~ 1 kHz over the entire lifespan of the fish is metabolically costly (Lewis et al. 2014; Markham et al. 2016). The neurons in this system also exhibited very small jitter, on the order of microseconds, indicating their high level of temporal accuracy. Typically, neuronal jitter is measured on the millisecond level, with some exceptions such as in *Eigenmannia*, where central neurons can have jitter on the order of 10 µs (Marsálek et al. 1997; Kawasaki 1993). The jitter of neurons in *Apteronotus* was found to be roughly half that in *Eigenmannia*, but further studies would be required to determine any physiological link between EOD frequency and jitter. *A. albifrons* potentially utilizes this 1:1 phase-locking with low jitter to maximize the advantages of the high-frequency EOD in electroreception.

MMN as a temporal processing center

We found MMN in *A. albifrons* to be a closed, unpaired nucleus which is specialized for the processing of temporal information. The first piece of evidence that MMN is specialized for temporal processing can be found in the presence of a high density of large diameter fibers, as well as large, adendritic somata (Fig. 6), two morphological features which often indicate phase-locking specialization and are seen in the phase comparator centers in *Eigenmannia*, as well as the pulse-type *Brachyhypopomus* (Carr et al. 1986b; Carr and Friedman 1999; Matsushita et al. 2013). These features are also prominent in the nucleus magnocellularis and nucleus laminaris of the barn owl, where inter-aural time differences are calculated, and precision phase-locking is paramount (Carr and Boudreau 1993). Second, within MMN we found large field potentials phase-locked to the EOD, as well as individual neurons phase-locked to the EOD, which responded to phase-modulated stimuli. Similar phase-locked field potentials can be found in lamina VI of TS in *Eigenmannia* as well as the medial zone of ELL in *Gymnarchus*, both of which are home to the phase-comparator circuit in those fishes (Kawasaki and Guo 1996). We also found that phase-locked field potentials followed a similar pathway as in *Brachyhypopomus*, where the field potentials are strongest in MMN and delayed relative to recordings in dLL (Fig. 5). Additionally, field potentials from the area of hMMN were slightly advanced relative to MMN (location *D* in Fig. 5), which, combined with the thick fibers seen in semi-thin sections (Fig. 6) as well as spherical cell labeling (Fig. 8), highlights hMMN as the point of entry into the nucleus for fibers carrying phase-locked information. The anatomical results indicate that the phase-comparison circuit in *A. albifrons* is likely the same as in other Gymnotiforms, and small cells are the likely phase-comparators.

Comparative anatomy

The current study first demonstrated phase-locked responses of individual neurons in the hypertrophied midbrain structure, MMN, which is found only in *A. albifrons* among wave-type high-frequency gymnotiform electric fishes (Szabo 1967). MMN is, however, common in pulse-type low-frequency gymnotiform electric fishes (Szabo and Fesseard 1974). The uniqueness of the temporal processing area in *A. albifrons* will be discussed below.

In *Eigenmannia*, much of the phase processing takes place in lamina VI of TS, where giant cells and small cells form a network for phase comparison (Carr et al. 1986a, b). The giant cells are arranged along this layer and can be seen throughout the width of TS. The phase processing area of *A. albifrons* appears closer to that of *Brachyhypopomus gauderio* and other pulse type Gymnotiforms, in that a separate closed nucleus has emerged that is dedicated to the coding of phase information (Matsushita et al. 2013). A similar nuclear structure is also seen in *A. leptorhynchus* and *Adontosternarchus* (unpublished observation), but there

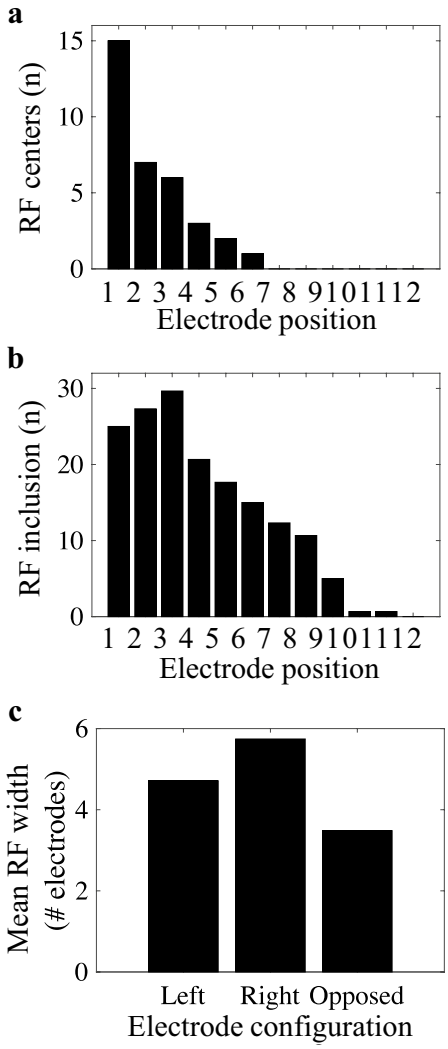

Fig. 10 Receptive field (RF) analysis data. **a** The number of receptive field centers found at each electrode position. Left-side, Right-side, and Opposite electrode configuration data are combined for each position. **b** The percentage of receptive field centers found on the left side or the right side of the body. The remaining percentage of neurons were stimulated by both sides equally. **c** The mean receptive field width given by the number of electrodes to which the neuron showed a response for left side, right side, and opposite electrode configurations

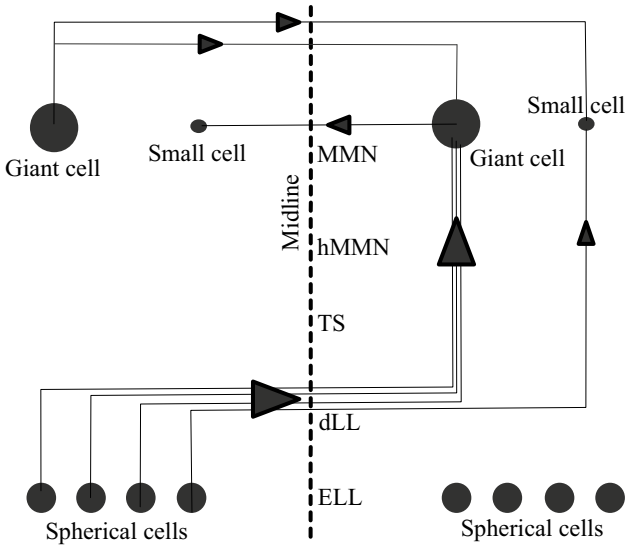

Fig. 11 Schematic drawing for the hypothetical phase-comparison circuit in *A. albifrons*. Spherical cells in ELL, which receive phase-locked inputs from electroreceptors, send axonal projections across the midline via dLL. The spherical cell projections then proceed through TS and enter MMN via hMMN. In MMN, spherical cell terminals synapse onto giant cell somata and small cell dendrites. Giant cells send axonal projections which cross the midline within MMN and synapse onto small cell somata. The small cells act as the phase-comparators, whose inputs are a spherical cell encoding phase from one part of the body, and a giant cell encoding phase from a different part of the body. Giant cell to giant cell connections are also seen in this fish

are some differences. In *A. leptorhynchus*, the nucleus is taller and more giant cell somata are visible. In some places it appears to divide TS into two halves as opposed to an unpaired midline structure as in *A. albifrons*. The structure in *Adontosternarchus* more closely resembles that of *A. leptorhynchus* as well.

The time-coding pathway of *A. albifrons* appears to be similar to other Gymnotiforms (Fig. 11). Spherical cells in the ELL send projections contralaterally to TS. In *A. albifrons*, the spherical cell projections terminate within MMN, much like the pear-shaped cells in *Brachyhypopomus*. In *Brachyhypopomus*, large cells of the MMN receive synaptic input from pear-shaped cells, and small cells receive input from both pear-shaped cells on the dendritic tufted tip and large cells on the soma (Matsushita et al. 2013). The tufted dendritic tip in *A. albifrons* is morphologically similar to that of *Brachyhypopomus*, in which spherical cells synaptically connected to the dendritic tip of the small cell (Matsushita et al. 2013). It is possible that the tufted dendritic would receive inputs from spherical cells also in *A. albifrons*, though further confirmation is required. On the other hand, the origin of the input to the somata in *Brachyhypopomus* as well as other studied species is a large cell (Matsushita et al. 2013; Matsushita and Kawasaki 2004), which may be also the case in *A. albifrons* (data not shown). This circuit is nearly identical in *Eigenmannia* also, except in *Eigenmannia* the circuit is contained within lamina 6 of TS, rather than a dedicated nucleus. In all three cases, the temporal processing pathway consists of three major cellular components: (1) a neuron in ELL which contralaterally projects to the temporal processing center in the midbrain, (2) neurons with large diameter somata which send their projections across the entire extent of the temporal processing center, and (3) small cells, which are known to function as phase comparators in *Eigenmannia*, but further studies

are required to confirm this in *A. albifrons*. A potential novelty in the *A. albifrons* circuit is giant cell to giant cell connectivity, which was observed in our experiments (Fig. 7) but is absent in the other fishes mentioned here. The major difference among these fishes arises from the location and neuroanatomy of the brain region where the phase comparator circuit appears to reside: a closed nucleus as in *Brachyhypopomus* and *A. albifrons*, or a laminated region within TS as in *Eigenmannia*. An advantage to the midline nucleus configuration in *A. albifrons* is the consolidation of neurons carrying phase information, thus minimizing the distance giant cell fibers have to travel. Additionally, the closed configuration of the nucleus isolates the midbrain phase-locked somata and fibers from fibers of other pathways, which may aid in maintaining the integrity of the system. The elucidation of why *Apteronotus* has different neuroanatomy for its phase processing area relative to other wave-type Gymnotiforms has yet to occur, but the high-frequency EOD may play a role.

Receptive fields

The receptive field data are consistent with previously published tuberous electroreceptor density data on *A. albifrons* (Szabo 1965; Carr et al. 1982). The head-biased electroreceptor density correlates with the majority of receptive field centers being found in and around the head region and anterior trunk. Motor behaviors related to electroreception in this fish may maximally stimulate receptors at the head and preclude the need for posterior representation of phase information, but future studies on the receptive fields of spherical cells in ELL would be needed to confirm the complete absence of phase representation from the posterior body. The concentration of receptive field centers away from the posterior trunk area indicates a disproportionate representation of afferent signals in MMN neurons. No correlation was found between recording electrode position and receptive field center location or receptive field size, but future studies will be required to determine the presence or absence of any topographic organization. It should be noted that Apteronotids also possess a dorsal filament, a thin, isolated structure located on the dorsal surface that contains many tuberous electroreceptors which morphologically resemble the timing specialized electroreceptors or T-units. It was previously suggested that this structure may play a role in phase processing (Franchina and Hopkins 1996). We searched for receptive fields along the entire horizontal plane of each fish, including the areas which contain the dorsal filament. Of the 35 neurons which met the inclusion criteria, only a few of them had receptive fields which extended to the dorsal filament, and none of them had a receptive field center in the area of the dorsal filament.

In conclusion, this paper documents phase processing neurons in the MMN of a high-frequency wave-type electric fish, *A. albifrons*. The MMN neurons of *A. albifrons* exhibit 1:1 phase-locked firing at frequencies exceeding 1 kHz in comparison to those found in MMN of other gymnotiform fishes which fire at much lower frequencies (< 100 Hz). The cytoarchitecture and gross anatomy of MMN in *A. albifrons*, however, are similar to the MMN of other gymnotiform fishes. The receptive fields of the phase-locked cells were heavily biased towards the head area, with no midbrain representation of the posterior half of the body. Future studies examining the receptive fields of spherical cells in ELL, as well as the targets of small cell fibers leaving MMN, will be advantageous for expanding our understanding of phase processing systems in very high frequency weakly electric fishes.

Declarations

Conflict of interest All authors declare that they have no conflicts of interest.

References

Bastian J, Chacron MJ, Maler L (2002) Receptive field organization determines pyramidal cell stimulus-encoding capability and spatial stimulus selectivity. J Neurosci 22(11):4577–4590. https://doi.org/10.1523/JNEUROSCI.22-11-04577.2002

Carr CE, Boudreau RE (1993) An axon with a myelinated initial segment in the bird auditory system. Brain Res 628(1–2):330–334. https://doi.org/10.1016/0006-8993(93)90975-s

Carr CE, Friedman MA (1999) Evolution of time coding systems. Neural Comput 11(1):1–20. https://doi.org/10.1162/089976699300016773

Carr CE, Maler L, Sas E (1982) Peripheral organization and central projections of the electrosensory nerves in gymnotiform fish. J Comp Neurol 211(2):139–153. https://doi.org/10.1002/cne.902110204

Carr CE, Heiligenberg W, Rose GJ (1986a) A time-comparison circuit in the electric fish midbrain. I. Behavior and physiology. J Neurosci 6(1):107–119. https://doi.org/10.1523/JNEUROSCI.06-01-00107.1986

Carr CE, Maler L, Taylor B (1986b) A time-comparison circuit in the electric fish midbrain. II. Functional morphology. J Neurosci 6(5):1372–1383. https://doi.org/10.1523/JNEUROSCI.06-05-01372.1986

Chacron MJ, Doiron B, Maler L, Longtin A, Bastian J (2003) Non-classical receptive field mediates switch in a sensory neuron's frequency tuning. Nature 423(6935):77–81. https://doi.org/10.1038/nature01590

Franchina CR, Hopkins CD (1996) The dorsal filament of the weakly electric Apteronotidae (Gymnotiformes; Teleostei) is specialized for electroreception. Brain Behav Evol 47(4):165–178. https://doi.org/10.1159/000113236

Gerstner W, Kreiter AK, Markram H, Herz AV (1997) Neural codes: firing rates and beyond. Proc Natl Acad Sci USA 94(24):12740–12741. https://doi.org/10.1073/pnas.94.24.12740

Guo YX, Kawasaki M (1997) Representation of accurate temporal information in the electrosensory system of the African electric fish, *Gymnarchus niloticus*. J Neurosci 17(5):1761–1768. https://doi.org/10.1523/JNEUROSCI.17-05-01761.1997

Kawasaki M (1993) Temporal hyperacuity in the gymnotiform electric fish, *Eigenmannia*. Ameri Zool 33:86–93

Kawasaki M (2009) Evolution of time-coding systems in weakly electric fishes. Zool Sci 26(9):587–599. https://doi.org/10.2108/zsj.26.587

Kawasaki M, Guo YX (1996) Neuronal circuitry for comparison of timing in the electrosensory lateral line lobe of the African wave-type electric fish *Gymnarchus niloticus*. J Neurosci 16(1):380–391. https://doi.org/10.1523/JNEUROSCI.16-01-00380.1996

Konishi M (1991) Deciphering the Brain's Codes. Neural Comput 3(1):1–18. https://doi.org/10.1162/neco.1991.3.1.1

Konishi M (2003) Coding of auditory space. Annu Rev Neurosci 26(1):31–55

Lewis JE, Gilmour KM, Moorhead MJ, Perry SF, Markham MR (2014) Action potential energetics at the organismal level reveal a trade-off in efficiency at high firing rates. J Neurosci 34(1):197–201. https://doi.org/10.1523/JNEUROSCI.3180-13.2014

Maler L (2009a) Receptive field organization across multiple electrosensory maps. I. Columnar organization and estimation of receptive field size. J Comp Neurol 516(5):376–393. https://doi.org/10.1002/cne.22124

Maler L (2009b) Receptive field organization across multiple electrosensory maps. II. Computational analysis of the effects of receptive field size on prey localization. J Comp Neurol 516(5):394–422. https://doi.org/10.1002/cne.22120

Markham MR, Ban Y, McCauley AG, Maltby R (2016) Energetics of sensing and communication in electric fish: a blessing and a curse in the Anthropocene? Integr Comp Biol 56(5):889–900. https://doi.org/10.1093/icb/icw104

Marsálek P, Koch C, Maunsell J (1997) On the relationship between synaptic input and spike output jitter in individual neurons. Proc Natl Acad Sci USA 94(2):735–740. https://doi.org/10.1073/pnas.94.2.735

Martinez D, Metzen MG, Chacron MJ (2016) Electrosensory processing in *Apteronotus albifrons*: implications for general and specific neural coding strategies across wave-type weakly electric fish species. J Neurophysiol 116(6):2909–2921. https://doi.org/10.1152/jn.00594.2016

Matsushita A, Kawasaki M (2004) Unitary giant synapses embracing a single neuron at the convergent site of time-coding pathways of an electric fish, *Gymnarchus niloticus*. J Comp Neurol 472(2):140–155. https://doi.org/10.1002/cne.11041

Matsushita A, Pyon G, Kawasaki M (2013) Time disparity sensitive behavior and its neural substrates of a pulse-type gymnotiform electric fish, *Brachyhypopomus gauderio*. J Comp Physiol A 199(7):583–599. https://doi.org/10.1007/s00359-012-0784-4

Nelson ME, Maciver MA (1999) Prey capture in the weakly electric fish *Apteronotus albifrons*: sensory acquisition strategies and electrosensory consequences. J Exp Biol 202(Pt 10):1195–1203

Réthelyi M, Szabo T (1973) A particular nucleus in the mesencephalon of weakly electric fish, *Gymnotus carapo,* Gymnotidae. I. Light microscopic structure. Exp Brain Res 17:229–241

Rose GJ, Heiligenberg W (1985) Structure and function of electrosensory neurons in the torus semicircularis of *Eigenmannia*: morphological correlates of phase and amplitude sensitivity. J Neurosci 5:2269–2280

Somjen G (1972) Sensory coding in the mammalian nervous system. Plenum, New York

Sullivan WE, Konishi M (1984) Segregation of stimulus phase and intensity coding in the cochlear nucleus of the barn owl. J Neurosci 4(7):1787–1799. https://doi.org/10.1523/JNEUROSCI.04-07-01787.1984

Szabo T (1965) Sense organs of the lateral line system in some electric fish of the *Gymnotidae*, *Mormyridae* and *Gymnarchidae*. J Morphol 117(2):229–249. https://doi.org/10.1002/jmor.1051170208

Szabo T (1967) Activity of peripheral and central neurons involved in electroreception. In: Cahn PH (ed) Lateral line detectors. Indiana Univ Press, Bloomington, pp 295–311

Szabo T, Fessard A (1974) Physiology of electroreceptors. In: Fessard A (ed) Handbook of sensory physiology III/3 electroreceptors and other specialized receptors in lower vertebrates. Springer, New York, pp 59–124